

# Compositional dependence of the apatite formation ability of Ti Zr alloys designed for hard tissue reconstruction

著者	Miyazaki Toshiki, Hosokawa Tomoya, Yokoyama Ken'ichi, Shiraishi Takanobu
journal or publication title	Journal of Materials Science: Materials in Medicine
volume	31
page range	110-1-110-8
year	2020-11-09
URL	<a href="http://hdl.handle.net/10228/00008523">http://hdl.handle.net/10228/00008523</a>

doi: <https://doi.org/10.1007/s10856-020-06448-9>

[Click here to view linked References](#)

1  
2  
3  
4  
5  
6  
7  
8  
9  
10  
11  
12  
13  
14  
15  
16  
17  
18  
19  
20  
21  
22  
23  
24  
25  
26  
27  
28  
29  
30  
31  
32  
33  
34  
35  
36  
37  
38  
39  
40  
41  
42  
43  
44  
45  
46  
47  
48  
49  
50  
51  
52  
53  
54  
55  
56  
57  
58  
59  
60  
61  
62  
63  
64  
65

1     **Compositional dependence of the apatite formation ability of Ti–Zr**  
2     **alloys designed for hard tissue reconstruction**

3  
4     Toshiki Miyazaki<sup>a</sup>, Tomoya Hosokawa<sup>a</sup>, Ken'ichi Yokoyama<sup>b</sup>, Takanobu Shiraishi<sup>c</sup>

5  
6     <sup>a</sup>Graduate School of Life Science and System Engineering, Kyushu Institute of  
7     Technology, Kitakyushu, Japan

8     <sup>b</sup>Department of Materials Science and Engineering, Kyushu Institute of Technology,  
9     Kitakyushu, Japan

10    <sup>c</sup>Graduate School of Biomedical Sciences, Nagasaki University, Nagasaki, Japan

11  
12    Corresponding author: Toshiki Miyazaki

13    Graduate School of Life Science and Systems Engineering, Kyushu Institute of  
14    Technology, 2-4, Hibikino, Wakamatsu-ku, Kitakyushu 808-0196, Japan

15    Tel./Fax: +81-93-695-6025

16    E-mail: tmiya@life.kyutech.ac.jp

17

1  
2  
3 **1 Abstract**  
4  
5  
6

7 2 Ti–Zr alloys are expected to be novel biomaterials with low stress shielding owing to  
8  
9  
10 3 their lower Young’s moduli than pure Ti. The drawback of metallic biomaterials is that  
11  
12  
13 4 their bone-bonding abilities are relatively low. NaOH and heat treatments have been  
14  
15  
16  
17 5 performed to provide Ti–50Zr with apatite-forming ability in the body environment,  
18  
19  
20  
21 6 which is essential for bone bonding. However, the systematic compositional dependence  
22  
23  
24 7 of apatite formation has not been revealed. In the present study, NaOH treatment of  
25  
26  
27  
28 8 Ti–Zr alloys with various compositions and bone-bonding abilities was assessed in vitro  
29  
30  
31  
32 9 by apatite formation in simulated body fluid (SBF). The corrosion current density in  
33  
34  
35 10 NaOH aqueous solution and the amount of Na incorporated into the surface tended to  
36  
37  
38  
39 11 decrease with increasing Zr content. The apatite-forming ability of the treated alloy  
40  
41  
42 12 significantly decreased when the Zr content was  $\geq 60$  atom%. This phenomenon is  
43  
44  
45 13 attributed to the (1) low OH content on the surface, (2) low Na incorporation into the  
46  
47  
48  
49 14 treated alloy surface, which enhances apatite formation, and (3) low ability of P  
50  
51  
52  
53 15 adsorption to the Ti–Zr alloy in SBF following Ca adsorption to trigger apatite  
54  
55  
56 16 nucleation. Although the adhesion of the titanate/zirconate layer formed on the surfaces  
57  
58  
59  
60  
61  
62  
63  
64  
65

1  
2  
3  
4  
5  
6  
7  
8  
9  
10  
11  
12  
13  
14  
15  
16  
17  
18  
19  
20  
21  
22  
23  
24  
25  
26  
27  
28  
29  
30  
31  
32  
33  
34  
35  
36  
37  
38  
39  
40  
41  
42  
43  
44  
45  
46  
47  
48  
49  
50  
51  
52  
53  
54  
55  
56  
57  
58  
59  
60  
61  
62  
63  
64  
65

1 to the substrates increased as Zr content increased, the adhesion between the apatite and  
2 the substrate was still low.

3 **Keywords:** Ti–Zr alloy, NaOH treatment, Apatite, Simulated body fluid, Hard tissue  
4 reconstruction

5

6 **Running Heads:** Compositional dependence of the apatite formation ability

7

1  
2  
3 **1. Introduction**  
4  
5  
6

7 2 Because metallic materials, such as Ti and its alloys, have high mechanical  
8  
9  
10 3 strength and fracture toughness, they are clinically applied to repair hard tissues, such as  
11  
12  
13 4 bone and joints, under high loaded conditions [1]. However, they have the drawback of  
14  
15  
16 5 poor bone-bonding ability leading to low long-term stability of fixation [2]. Formation  
17  
18  
19 6 of bone-like apatite in a body fluid environment is necessary for the material to bond to  
20  
21  
22 7 bone [3]. This type of apatite formation is known to be reproduced even in simulated  
23  
24  
25 8 body fluid (SBF) that mimics the human body fluid composition [4]. Various surface  
26  
27  
28 9 modifications of Ti, such as NaOH treatment [5], hydrogen peroxide treatment [6],  
29  
30  
31 10 anodic oxidation [7], and hydrothermal treatment [8,9], have been proposed to improve  
32  
33  
34 11 the bone-bonding ability of Ti.  
35  
36  
37  
38  
39  
40  
41

42 12 Ti–Zr alloys are expected to be novel biomaterials with low stress shielding owing  
43  
44  
45 13 to their lower Young’s moduli than pure Ti. It has mechanical strength comparable to  
46  
47  
48 14 commercialized Ti-29Nb-13Ta-4.6Zr alloy with low Young’s moduli [10,11]. Also,  
49  
50  
51 15 Ti–Zr binary system gives solid solution at any composition [12], therefore the galvanic  
52  
53  
54 16 corrosion in body environment can be suppressed. Shiraishi *et al.* [13] fabricated Ti–Zr  
55  
56  
57  
58  
59  
60  
61  
62  
63  
64  
65

1 alloys with various compositions and evaluated their mechanical properties, and they  
2 found that the Young's modulus decreases to 90 GPa at Ti-60 atom% Zr. It has also  
3 been reported that pure Zr [14] and Ti-50 atom% Zr [15,16] subjected to NaOH  
4 treatment (and subsequent heat treatment for some metals) shows apatite-forming  
5 ability in SBF. However, the systematic compositional dependence of apatite formation  
6 has not been reported.

7 In this study, Ti-Zr alloys with different compositions were treated with NaOH  
8 aqueous solution, and their apatite-formation abilities were investigated *in vitro* using  
9 SBF. The surface structural changes caused by NaOH treatment were analyzed  
10 spectroscopically and electrochemically, and their affect on apatite formation was  
11 investigated.

## 12

### 13 **2. Materials and methods**

#### 14 2.1. Specimen preparation

15 The Ti-Zr alloys, as well as pure Ti and Zr, were prepared by the arc-melting  
16 method. NaOH and the reagents used to prepare SBF were purchased from Nacalai

1  
2  
3 1 Tesque Inc. (Kyoto, Japan).  $\text{NH}_4\text{Cl}$ ,  $\text{ZnCl}_2$ ,  $\text{NH}_3$ , and  $\text{HNO}_3$  aqueous solutions were  
4  
5  
6  
7 2 purchased from FUJIFILM Wako Pure Chemical Co. (Osaka, Japan).  
8  
9

10 3 The alloy substrates with dimensions of  $5 \text{ mm} \times 5 \text{ mm} \times 1 \text{ mm}$  were polished  
11  
12  
13  
14 4 with #500 SiC paper. Hereafter, the Ti–Zr alloys containing  $x$  atom% Zr are denoted  
15  
16  
17 5  $\text{Ti-}x\text{Zr}$  ( $x = 20\text{--}80$ ). Each substrate was then soaked in 5 mL of 5 M NaOH aqueous  
18  
19  
20  
21 6 solution and shaken in a water bath (H-10, Taitec Co., Saitama, Japan) at  $60 \text{ }^\circ\text{C}$  and 120  
22  
23  
24 7 strokes/min for 1 day. The substrates were then removed from solution, gently washed  
25  
26  
27  
28 8 with ultrapure water, and dried at  $60 \text{ }^\circ\text{C}$ .  
29  
30

## 31 32 9 33 34 35 10 2.2. Soaking in SBF

36  
37  
38 11 The treated substrates were soaked in 30 mL of SBF containing 142.0 mM  $\text{Na}^+$ ,  
39  
40  
41  
42 12 5.0 mM  $\text{K}^+$ , 2.5 mM  $\text{Mg}^{2+}$ , 147.8 mM  $\text{Cl}^-$ , 4.2 mM  $\text{HCO}_3^-$ , 1.0 mM  $\text{HPO}_4^{2-}$ , and 0.5  
43  
44  
45 13 mM  $\text{SO}_4^{2-}$  at  $36.5 \text{ }^\circ\text{C}$  for various periods. The pH of the solution was buffered at 7.40  
46  
47  
48  
49 14 by 50 mM tris(hydroxymethyl)aminomethane and an appropriate amount of HCl. The  
50  
51  
52  
53 15 SBF was prepared according to the literature [4]. After soaking, the substrates were  
54  
55  
56 16 removed from the SBF and then subjected to ultrasonic cleaning with ultrapure water  
57  
58  
59  
60  
61  
62  
63  
64  
65

1  
2  
3 1 for 30 min to remove excess water-soluble salts on their surfaces.  
4  
5  
6

7 2  
8  
9  
10 3 2.3. Characterization  
11  
12

13  
14 4 The surface structural changes of the substrates were characterized by scanning  
15  
16  
17 5 electron microscopy (SEM, Model S-3500N, Hitachi Co., Tokyo, Japan), energy  
18  
19  
20  
21 6 dispersive X-ray spectroscopy (EDX, Model EX-400, Horiba Co., Kyoto, Japan), and  
22  
23  
24 7 thin-film X-ray diffraction (TF-XRD, MXP3V, Mac Science Ltd., Yokohama, Japan). In  
25  
26  
27  
28 8 the TF-XRD experiments, CuK $\alpha$  X-ray with voltage and current of 30 kV and 40 mA,  
29  
30  
31  
32 9 respectively, was used and the incident beam was fixed at 1° to the surface of each  
33  
34  
35 10 substrate and the scan rate was 0.02°·s<sup>-1</sup>. In EDX, the atomic ratio of each element was  
36  
37  
38 11 calculated from the peak area in the EDX spectrum by using ZAF correction method.  
39  
40  
41

42 12 Three points were measured for each specimen. Specimens for cross-sectional  
43  
44  
45 13 observation were prepared by embedding in light-curing resin (Technovit 4071, KulZer  
46  
47  
48  
49 14 GmbH, Hanau, Germany), cutting and polishing with #80, #120, #240, #500 and #1000  
50  
51  
52 15 SiC paper.

53  
54  
55  
56 16 Rate of corrosion corresponding to surface oxide formation was evaluated by  
57  
58  
59  
60  
61  
62  
63  
64  
65



1 polarization test. It was performed in 1 M NaOH aqueous solution using a potentiostat  
2  
3  
4  
5  
6  
7 (HA-151A, Hokuto Denko Co., Tokyo, Japan) equipped with a saturated calomel  
8  
9  
10 electrode as the reference electrode and a Pt electrode as the counter electrode [17]. The  
11  
12  
13  
14 specimens were embedded in acrylic resin and the cross-section was abraded with #120,  
15  
16  
17 #240, and #500 SiC paper. In the polarization test, the sample was first immersed in 1  
18  
19  
20  
21 M NaOH aqueous solution for 10 min, and the approximate corrosion potential was  
22  
23  
24  
25 measured. The specimens were then polarized from the corrosion potential to the anode  
26  
27  
28 (+1.5 V) or cathode direction (-1.5 V) at a sweep rate of 20 mV min<sup>-1</sup>. Measurement  
29  
30  
31  
32 was performed once for each specimen.

33  
34  
35 Surface OH formation by NaOH treatment is reported to govern the apatite  
36  
37  
38 formation in body environment [5]. Therefore, the concentration of surface OH groups  
39  
40  
41  
42 was determined by formation of a zinc complex [18]. The Zn solution was prepared by  
43  
44  
45  
46 mixing 500 mL of 4 M NH<sub>4</sub>Cl and 250 mL of 0.4 M ZnCl<sub>2</sub>, adjusting the pH to 6.9 with  
47  
48  
49  
50 25% NH<sub>3</sub> aqueous solution, and finally adjusting the volume to 1000 mL. Each  
51  
52  
53  
54 specimen was soaked in 150 mL of the Zn solution for 5 min and washed with 150 mL  
55  
56  
57 of ultrapure water for 10 min. The washing operation was repeated three times. Each  
58  
59  
60  
61  
62  
63  
64  
65

1 specimen was then dried for 1 h and soaked in 100 mL of 2.42 M HNO<sub>3</sub> aqueous  
2 solution for 10 min. The Zn concentration in the HNO<sub>3</sub> solution was measured by  
3 inductively coupled plasma atomic emission spectroscopy (ICPE-9800, Shimadzu Co.,  
4 Kyoto, Japan). The surface active OH concentration ( $C_{OH}$ ) was calculated by the  
5 following equation [18]:

$$C_{OH} = \frac{2C_{Zn}VA}{S} \quad (1)$$

6 where  $C_{Zn}$ ,  $V$ ,  $S$ , and  $A$ , are the Zn concentration in the HNO<sub>3</sub> solution (mM), volume of  
7 the HNO<sub>3</sub> solution (L), surface area of the specimen (mm<sup>2</sup>), and Avogadro number (6.02  
8  $\times 10^{23}$ ), respectively. Measurement was performed three to six times for each specimen.

9  
10 The adhesive strength of the apatite layer formed on the specimens was measured  
11 by peeling-off test regulated in JIS K 5600. An adhesive tape (CT-15105P, NICHIBAN  
12 Co., Ltd., Tokyo, Japan) was attached on the specimens and detached. This operation  
13 was repeated 5 times.

### 14 15 **3. Results**

16 SEM images of the specimen surfaces before and after NaOH treatment are shown

1  
2  
3 in Fig. 1. Before treatment, only polishing scratches were observed in any of the  
4  
5  
6  
7 specimens. After NaOH treatment, pure Ti and Ti-20Zr showed a network structure  
8  
9  
10 composed of flake-like particles of less than 1  $\mu\text{m}$  in size. When the Zr content was 40  
11  
12  
13 or 50 atom%, formation of a layer without a network structure was observed. Above 50  
14  
15  
16 atom% Zr, no layer formed and polishing scratches were observed, similar to before  
17  
18  
19  
20  
21 treatment.

22  
23  
24 The amounts of OH groups on the specimen surfaces before and after NaOH  
25  
26  
27 treatment, which were determined by Zn complex formation method, are shown in Fig.  
28  
29  
30  
31  
32 2. For the untreated specimens, the OH amount was about  $1 \times 10^{16} \text{ mm}^{-2}$  irrespective of  
33  
34  
35 the Zr content. In contrast, the OH amount on the NaOH-treated Ti specimen was about  
36  
37  
38  
39  $4 \times 10^{16} \text{ mm}^{-2}$  and it tended to decrease with increasing Zr content. The OH amount of  
40  
41  
42 Ti-20Zr was lower than that of Ti and Ti-40Zr. Detailed reason is not clear at present.  
43  
44  
45 However, judging from the results that Na content is almost the same and morphology  
46  
47  
48  
49 of the former was a little different from the latter, difference in OH amount may be  
50  
51  
52 attributed to specific surface area. When the Zr content was  $\geq 70$  atom%, the OH amount  
53  
54  
55  
56  
57 was almost the same as that of the untreated specimens.  
58  
59  
60  
61  
62  
63  
64  
65

1           The relationship between the Na/(Ti+Zr) ratio on the NaOH-treated specimen  
2 surface and the Zr content, which were determined by EDX quantitative analyses, is  
3 shown in Figure 3. The Na/(Ti+Zr) ratio was 0.12 for pure Ti. With increasing Zr  
4 content, the Na/(Ti+Zr) ratio increased until 40 atom% Zr and then decreased. Na was  
5 hardly detected at Zr content  $\geq 80$  atom%.

6           The relationship between the corrosion current density of the specimen in 1 M  
7 NaOH aqueous solution and the Zr content is shown in Figure 4. The corrosion current  
8 density monotonically decreased with increasing Zr content, indicating that the  
9 corrosion resistance against NaOH increased.

10          The TF-XRD patterns of the untreated and NaOH-treated specimens are shown in  
11 Fig. 5. Only the diffraction peaks assigned to the alloys were observed for the untreated  
12 specimen. The diffraction angle shifted to lower angle with increasing Zr content. This  
13 agrees with the Ti–Zr phase diagram showing an all-proportional solid solution [12].  
14 After NaOH treatment, peaks assigned to crystalline zirconium titanate were only  
15 observed for Ti–60Zr and Ti–70Zr.

16          SEM-EDX profiles of cross-sections of NaOH-treated specimens. in Fig. 6.

1  
2  
3 1 Concentration gradient of change Ti and Zr increased with increase in Zr content,  
4  
5  
6  
7 2 suggesting that the thickness of the surface oxide layer is decreased.  
8  
9

10 3 SEM images of the specimen surfaces after NaOH treatment and subsequent  
11  
12  
13  
14 4 immersion in SBF for 7 days are shown in Fig. 7. Spherical particles formed on the  
15  
16  
17 5 samples with Zr content  $\leq 50$  atom%. In the TF-XRD patterns of the specimens shown  
18  
19  
20  
21 6 in Fig. 8, broad peaks assigned to poorly crystalline apatite (JCPDS#09-0432) are  
22  
23  
24  
25 7 observed at  $2\theta = 26^\circ$  and  $32^\circ$  for Zr content  $\leq 50$  atom%. This means that the formed  
26  
27  
28 8 spherical particles were poorly crystalline apatite.  
29  
30

31 9 The (Ca or P)/(Ti+Zr) molar ratios of the specimen surfaces with Zr content of  
32  
33  
34  
35 10  $\geq 60$  atom% after soaking in SBF for 7 days, where no apatite formed, are shown in Fig.  
36  
37  
38  
39 11 9. They were determined by EDX quantitative analyses. Both Ca and P were detected  
40  
41  
42 12 for 60 atom% Zr, while only Ca was detected for  $\geq 70$  atom% Zr.  
43  
44

45 13 Figure 10 shows SEM images of the specimen surfaces after NaOH treatment and  
46  
47  
48  
49 14 subsequent immersion in SBF for 7 days, which were attached and detached with an  
50  
51  
52  
53 15 adhesive tape 5 times. Surface titanate/zirconate layer as well as the apatite particles  
54  
55  
56 16 was peeled-off for pure Ti and 20 atom% Zr, while only the apatite particles for 40  
57  
58  
59  
60  
61  
62  
63  
64  
65

1  
2  
3 1 atom% Zr and 50 atom% Zr.  
4  
5  
6

7 2  
8  
9  
10 3 **4. Discussion**  
11

12  
13  
14 4 The thickness of the surface reaction product significantly decreased at high Zr  
15  
16  
17 5 content (>50 atom% Zr). This is attributed to reduction of the reactivity against NaOH  
18  
19  
20  
21 6 aqueous solution. This assumption is supported by the data showing reduction of the  
22  
23  
24  
25 7 corrosion current and OH concentration (see Figs. 2 and 4).  
26  
27

28 8 The surface phases on the alloys produced by NaOH treatment significantly  
29  
30  
31 9 varied depending on the Zr content. The surface phases on the alloys predicted from the  
32  
33  
34  
35 10 data in Figs. 2, 3, and 5 are given in Table 1. According to the Pourbaix diagram,  
36  
37  
38 11  $\text{HTiO}_3^-$  and  $\text{HZrO}_3^-$  are stable chemical species around pH 14.7, corresponding to 5 M  
39  
40  
41  
42 12 NaOH, meaning that sodium (hydrogen) titanate/zirconate favorably forms [19].  
43  
44  
45  
46 13 However, the present result showing no Na incorporation into NaOH-treated Zr is  
47  
48  
49 14 different from that predicted from the Pourbaix diagram (see Fig. 3). It has been  
50  
51  
52  
53 15 reported that although Na is observed on the top surface of Zr treated with 6.1 M NaOH  
54  
55  
56 16 at 50 °C by X-ray photoelectron spectroscopy (XPS), it disappears after  $\text{Ar}^+$  sputtering  
57  
58  
59  
60  
61  
62  
63  
64  
65

1  
2  
3 1 for 6 s [20]. Therefore, Na may exist only on the top surface of the present specimens.  
4  
5

6  
7 2 However, from the fact that Zr has a significantly lower corrosion rate than Ti in NaOH  
8  
9  
10 3 solution [20], zirconia hydrogel would be the dominant phase. This is consistent with  
11  
12  
13  
14 4 the report by Uchida *et al.* [14], where zirconia hydrogel formed after 20 M NaOH  
15  
16  
17 5 treatment.  
18  
19  
20

21 6 When the Zr content exceeded 50 atom%, the apatite-forming ability significantly  
22  
23  
24 7 decreased (see Figs. 7 and 8). From the result that the specimens formed with the  
25  
26  
27  
28 8 zirconium titanate phase did not precipitate apatite, the zirconium titanate phase would  
29  
30  
31 9 not contribute to apatite formation. Ti–OH [21] and Zr–OH [22] groups trigger  
32  
33  
34  
35 10 heterogeneous apatite nucleation in the body environment. Therefore, the decrease in  
36  
37  
38  
39 11 the OH amount shown in Fig. 2 would suppress apatite formation. In addition, for  
40  
41  
42 12 NaOH-treated Ti, Na<sup>+</sup> released from the surface sodium titanate is known to increase  
43  
44  
45  
46 13 the pH of SBF by ion exchange with H<sub>3</sub>O<sup>+</sup> and the supersaturation degree with respect  
47  
48  
49 14 to apatite, leading to enhancement of apatite formation [5]. In this study, all the  
50  
51  
52 15 specimens showed pH increase by 0.1 to 0.17 after soaking in SBF for 1 day (Data not  
53  
54  
55  
56 16 shown). In the case of the alloys with high Zr content, judging from the result that Na is  
57  
58  
59  
60  
61  
62  
63  
64  
65

1  
2  
3 1 hardly incorporated, pH increase would be attributed to another factor such as  
4  
5  
6  
7 2 dissolution of zirconium hydroxide on the surfaces [23]. However, the present results  
8  
9  
10 3 indicate that pH increase do not contribute to the apatite formation at high Zr content.

11  
12  
13  
14 4 Adsorption of P was not observed for the alloys that did not form apatite (see Fig.  
15  
16  
17 5 8). Hanawa and co-workers [24,25] investigated the surface structural changes of the  
18  
19  
20  
21 6 surfaces of pure Ti, pure Zr, and Ti–Zr alloys in Hanks’ solution by XPS, and they  
22  
23  
24  
25 7 found that pure Zr and Ti–Zr alloys with high Zr content adsorbed P but not Ca.

26  
27  
28 8 However, such zirconium phosphate was not detected for the present specimens by  
29  
30  
31  
32 9 EDX or XRD. This may be because analytical method or chemical state of surface  
33  
34  
35 10 zirconia is different. In addition, zirconia hydrogel produced by the sol–gel method is

36  
37  
38  
39 11 known to have the ability of Ca adsorption [26]. This means that the ion adsorption  
40  
41  
42  
43 12 behavior on the passive oxide film on the metal surface and the sol–gel-derived metal  
44  
45  
46  
47 13 oxide hydrogel is different, and the adsorption behavior on the surfaces of the present  
48  
49  
50  
51  
52  
53 14 alloys is relatively close to the latter. Apatite nucleation on NaOH- and heat-treated Ti in  
54  
55  
56  
57 15 SBF is known to proceed by Ca adsorption followed by P adsorption [27]. It has also  
58  
59  
60  
61  
62  
63 16 been reported that if Ca is adsorbed on zirconia hydrogel in advance, the P adsorption



1 capacity increases [26]. Therefore, the apatite-forming ability may be improved on the  
2 alloys with high Zr content by appropriate control of the state of Ca adsorption.

3         The surface potential is also an important factor that governs the apatite-forming  
4 ability. Hashimoto *et al.* [28] investigated apatite formation on Ti metal heat treated in  
5 various atmospheres, and they found that a highly negatively ( $-30$  to  $-15$  mV) or  
6 positively ( $10$  to  $15$  mV) charged sample tended to form a large amount of apatite. In  
7 contrast, the Ti–Hf alloy formed with hafnium titanate with a highly negative zeta  
8 potential of about  $-40$  mV did not form apatite [29]. This means that the surface charge  
9 suitable for induction of apatite formation is different depending on the substrate. In  
10 future, control of the surface potential should also be investigated.

11         It was found that the adhesion of the titanate/zirconate layer formed on the  
12 surfaces to the substrates increased as Zr content increased. Considering that the  
13 concentration gradient becomes gentle as Zr content increases, it is assumed that the  
14 stress concentration is suppressed by the formation of the graded structure. However,  
15 even in the alloys with high Zr content, the adhesion between the apatite and the  
16 substrate was low. This is probably because the alloys with high Zr content had a

1 smooth surface after NaOH treatment as shown in Fig. 1, and had little mechanical  
2 locking with the apatite. Kim *et al.* reported that heating at 600°C following NaOH  
3 treatment is effective for improving the adhesion of surface titanate layer to Ti substrate  
4 [30]. However, in this study, the apatite-forming ability was lost for all the specimens  
5 after the heat treatment at 600°C (Data not shown). Also, alpha-beta phase transition  
6 may occur around 600 to 800°C [12], which deteriorate mechanical properties of the  
7 alloys. It is necessary to pursue optimal heat treatment conditions that maintain the  
8 apatite-forming ability.

## 10 5. Conclusions

11 We have found that the apatite-forming ability of NaOH-treated Ti–Zr alloys in  
12 SBF is highly dependent on the Zr content. Namely, high Zr content significantly  
13 suppresses the apatite-forming ability. This phenomenon is attributed to reduction in the  
14 reaction rate in NaOH aqueous solution at high Zr content and the low potential for P to  
15 adsorb in SBF. In future, enhancement of the apatite-forming ability of Ti–60Zr is  
16 required, because it is has the lowest Young’s modulus among the Ti–Zr alloys.

1  
2  
3  
4  
5  
6  
7  
8  
9  
10  
11  
12  
13  
14  
15  
16  
17  
18  
19  
20  
21  
22  
23  
24  
25  
26  
27  
28  
29  
30  
31  
32  
33  
34  
35  
36  
37  
38  
39  
40  
41  
42  
43  
44  
45  
46  
47  
48  
49  
50  
51  
52  
53  
54  
55  
56  
57  
58  
59  
60  
61  
62  
63  
64  
65

1

2 **Acknowledgments**

3 The authors thank Ms. Akiko Nomura and Mr. Kazuo Obara of the Institute for  
4 Materials Research, Tohoku University, Sendai, Japan for their assistance with sample  
5 alloy preparation. We thank Tim Cooper, PhD, from Edanz Group  
6 ([www.edanzediting.com/ac](http://www.edanzediting.com/ac)) for editing a draft of this manuscript.

7

8 **References**

- 9 1. Breme J, Biehl V. Metallic Biomaterials. Black J, Hastings G, editors. Handbook of  
10 Biomaterial Properties, London: Chapman & Hall; 1998:135-213.
- 11 2. Yan WQ, Nakamura T, Kobayashi M, Kim HM, Miyaji F, Kokubo T. Bonding of  
12 chemically treated titanium implants to bone. J Biomed Mater Res  
13 1997;37:267-275.
- 14 3. Kokubo T, Kim HM, Kawashita M. Novel bioactive materials with different  
15 mechanical properties. Biomaterials 2003;24:2161-2175.
- 16 4. Cho SB, Kokubo T, Nakanishi K, Soga N, Ohtsuki C, Nakamura T, Kitsugi T,

1  
2  
3  
4  
5  
6  
7  
8  
9  
10  
11  
12  
13  
14  
15  
16  
17  
18  
19  
20  
21  
22  
23  
24  
25  
26  
27  
28  
29  
30  
31  
32  
33  
34  
35  
36  
37  
38  
39  
40  
41  
42  
43  
44  
45  
46  
47  
48  
49  
50  
51  
52  
53  
54  
55  
56  
57  
58  
59  
60  
61  
62  
63  
64  
65

1 Yamamuro. Dependence of Apatite Formation on Silica Gel on Its Structure: Effect  
2 of Heat Treatment. *J Am Ceram Soc* 1995;78:1769-1774.

3 5. Kim HM, Miyaji F, Kokubo T, Nakamura T. Preparation of bioactive Ti and its  
4 alloys via simple chemical surface treatment. *J Biomed Mater Res*  
5 1996;32:409-417.

6 6. Wang XX, Hayakawa S, Tsuru K, Osaka A. A comparative study of in vitro apatite  
7 deposition on heat-, H<sub>2</sub>O<sub>2</sub>-, and NaOH-treated titanium surfaces. *J Biomed Mater*  
8 *Res* 2001;54:172-178.

9 7. Yang BC, Uchida M, Kim HM, Zhang Z, Kokubo T. Preparation of bioactive  
10 titanium metal via anodic oxidation treatment. *Biomaterials* 2004;25:1003–1010.

11 8. Nakagawa M, Zhang L, Udoh K, Matsuya S, Ishikawa K. Effects of hydrothermal  
12 treatment with CaCl<sub>2</sub> solution on surface property and cell response of titanium  
13 implants. *J Mater Sci Mater Med* 2005;16:985–991.

14 9. Kawashita M, Matsui N, Miyazaki T, Kanetaka H. Effect of autoclave and hot  
15 water treatments on surface structure and in vitro apatite-forming ability of NaOH-  
16 and heat-treated bioactive titanium metal. *Mater Trans* 2013;54:811–816.

1  
2  
3  
4  
5  
6  
7  
8  
9  
10  
11  
12  
13  
14  
15  
16  
17  
18  
19  
20  
21  
22  
23  
24  
25  
26  
27  
28  
29  
30  
31  
32  
33  
34  
35  
36  
37  
38  
39  
40  
41  
42  
43  
44  
45  
46  
47  
48  
49  
50  
51  
52  
53  
54  
55  
56  
57  
58  
59  
60  
61  
62  
63  
64  
65

10. Niinomi M. Recent research and development in titanium alloys for biomedical applications and healthcare goods. *Sci Tech Adv Mater* 2003;4:445–454.

11. Ho WF, Chen WK, Wu SC, Hsu HC. Structure, mechanical properties, and grindability of dental Ti-Zr alloys. *J Mater Sci Mater Med* 2008;19:3179-3186.

12. Hari Kumar KC, Wollants P, Delacy L. Thermodynamic assessment of the Ti-Zr system and calculation of the Nb-Ti-Zr phase diagram. *J Alloys Compd* 1994;206:121-127.

13. Shiraishi T, Yubuta K, Shishido T, Shinozaki N. Elastic properties of as-solidified Ti-Zr binary alloys for biomedical applications. *Mater Trans* 2016;57:1986-1992.

14. Uchida M, Kim HM, Miyaji F, Kokubo T, Nakamura T. Apatite formation on zirconium metal treated with aqueous NaOH. *Biomaterials* 2002;23:313-317.

15. Chen X, Nouri A, Lin YJ, Hodgson PD, Wen C. Effect of surface roughness of Ti, Zr, and TiZr on apatite precipitation from simulated body fluid. *Biotech Bioeng* 2008;101:378–387.

16. Chen X, Li Y, Hodgson PD, Wen C. In vitro behavior of human osteoblast-like cells (SaOS2) cultured on surface modified titanium and titanium–zirconium alloy.

1  
2  
3  
4  
5  
6  
7  
8  
9  
10  
11  
12  
13  
14  
15  
16  
17  
18  
19  
20  
21  
22  
23  
24  
25  
26  
27  
28  
29  
30  
31  
32  
33  
34  
35  
36  
37  
38  
39  
40  
41  
42  
43  
44  
45  
46  
47  
48  
49  
50  
51  
52  
53  
54  
55  
56  
57  
58  
59  
60  
61  
62  
63  
64  
65

1 Mater Sci Eng C 2011;31:1545-1552.

2 17. Miyazaki T, Sasaki T, Shirosaki Y, Yokoyama K, Kawashita M. Effect of  
3 metallographic structure and machining process on the apatite-forming ability of  
4 sodium hydroxide- and heat-treated titanium. Bio-Med Mater Eng  
5 2018;29:109–118.

6 18. Sakamoto H, Hirohashi Y, Saito H, Doi H, Tsutsumi Y, Suzuki Y, Noda K, Hanawa  
7 T. Effect of active hydroxyl groups on the interfacial bond strength of titanium with  
8 segmented polyurethane through  $\gamma$ -mercapto propyl trimethoxysilane. Dent Mater J  
9 2008;27:81-92.

10 19. Pourbaix M. Atlas of Electrochemical Equilibria in Aqueous Solutions. Houston:  
11 National Association of Corrosion Engineers; 1974.

12 20. Motooka T, Yamamoto M. Corrosion behavior of Zr, Ti, Ta and Nb in sodium  
13 hydroxide solutions. Zairyo-to-Kankyo 2011;60:394-401 (in Japanese).

14 21. Li P, Ohtsuki C, Kokubo T, Nakanishi K, Soga N, de Groot K. The role of hydrated  
15 silica, titania, and alumina in inducing apatite on implants. J Biomed Mater Res  
16 1994;28:7-15.

1  
2  
3  
4  
5  
6  
7  
8  
9  
10  
11  
12  
13  
14  
15  
16  
17  
18  
19  
20  
21  
22  
23  
24  
25  
26  
27  
28  
29  
30  
31  
32  
33  
34  
35  
36  
37  
38  
39  
40  
41  
42  
43  
44  
45  
46  
47  
48  
49  
50  
51  
52  
53  
54  
55  
56  
57  
58  
59  
60  
61  
62  
63  
64  
65

1 22. Uchida M, Kim HM, Kokubo T, Miyaji F, Nakamura T. Bonelike apatite formation  
2 induced on zirconia gel in a simulated body fluid and its modified solutions. J Am  
3 Ceram Soc 2001;84:2041-2044.

4 23. Kobayashi T, Sasaki T, Takagi I, Moriyama H. Solubility of zirconium (IV) hydrous  
5 oxides, J Nucl Sci Tech 2007;44:90-94.

6 24. Hanawa T, Okuno O, Hamanaka H. Compositional change in surface of Ti-Zr  
7 alloys in artificial bioliquid. J Jpn Inst Metals 1992;56:1168-1173 (in Japanese).

8 25. Tsutsumi Y, Nishimura D, Doi H, Nomura N, Hanawa T. Difference in surface  
9 reactions between titanium and zirconium in Hanks' solution to elucidate  
10 mechanism of calcium phosphate formation on titanium using XPS and cathodic  
11 polarization. Mater Sci Eng C 2009;29:1702-1708.

12 26. J. Lin, Y. Zhan, H. Wang, M. Chu, C. Wang, Y. He, X. Wang, Effect of calcium ion  
13 on phosphate adsorption onto hydrous zirconium oxide, Chem. Eng. J. 309 (2017)  
14 118-129. DOI: 10.1016/j.cej.2016.10.001

15 27. Takadama H, Kim HM, Kokubo T, Nakamura T. An X-ray photoelectron  
16 spectroscopy study of the process of apatite formation on bioactive titanium metal.

1  
2  
3  
4  
5  
6  
7  
8  
9  
10  
11  
12  
13  
14  
15  
16  
17  
18  
19  
20  
21  
22  
23  
24  
25  
26  
27  
28  
29  
30  
31  
32  
33  
34  
35  
36  
37  
38  
39  
40  
41  
42  
43  
44  
45  
46  
47  
48  
49  
50  
51  
52  
53  
54  
55  
56  
57  
58  
59  
60  
61  
62  
63  
64  
65

1 J Biomed Mater Res 2001;55:185-193.

2 28. Hashimoto M, Ogawa T, Kitaoka S, Muto S, Furuya M, Kanetaka H, Abe M,  
3 Yamashita H. Control of surface potential and hydroxyapatite formation on TiO<sub>2</sub>  
4 scales containing nitrogen-related defects. Acta Mater 2018;155:379-385.

5 29. Miyazaki T, Sueoka M, Shirosaki Y, Shinozaki N, Shiraishi T. Development of  
6 hafnium metal and titanium-hafnium alloys having apatite-forming ability by  
7 chemical surface modification. J Biomed Mater Res Part B Appl Biomater  
8 2018;106B:2519–2523.

9 30. Kim HM, Miyaji F, Kokubo T, Nakamura T. Effect of heat treatment on  
10 apatite-forming ability of Ti metal induced by alkali treatment. J Mater Sci Mater  
11 Med 1997;8:341–347.



**Table 1** Predicted surface phases formed on the alloys by NaOH treatment

Zr content in atom%	Surface phase
0	Sodium titanate hydrogel
20, 40	Sodium titanate/zirconate hydrogel
60	Sodium titanate/zirconate hydrogel, Crystalline ZrTiO <sub>4</sub>
70	Zirconia/titania hydrogel, Crystalline ZrTiO <sub>4</sub>
80	Zirconia/titania hydrogel
100	Zirconia hydrogel

1  
2  
3  
4  
5  
6  
7  
8  
9  
10  
11  
12  
13  
14  
15  
16  
17  
18  
19  
20  
21  
22  
23  
24  
25  
26  
27  
28  
29  
30  
31  
32  
33  
34  
35  
36  
37  
38  
39  
40  
41  
42  
43  
44  
45  
46  
47  
48  
49  
50  
51  
52  
53  
54  
55  
56  
57  
58  
59  
60  
61  
62  
63  
64  
65

1 **Figure captions**

2 **Figure 1** SEM images of the specimen surfaces before and after NaOH treatment.

3 **Figure 2** Relationships between the amounts of OH groups on the specimen surfaces  
4 before and after NaOH treatment and the Zr content, which were determined by Zn  
5 complex formation method (n=3 for untreated sample and n=6 for treated sample).

6 **Figure 3** Relationship between the Na/(Ti+Zr) molar ratio on the NaOH-treated  
7 specimen surface and the Zr content, which was determined by EDX quantitative  
8 analyses (n=3).

9 **Figure 4** Relationship between the corrosion current density of the specimen in 1 M  
10 NaOH aqueous solution and the Zr content (n=1).

11 **Figure 5** TF-XRD patterns of the untreated and NaOH-treated specimens.

12 **Figure 6** SEM-EDX profiles of cross-sections of NaOH-treated specimens.

13 **Figure 7** SEM images of the specimen surfaces after NaOH treatment and subsequent  
14 immersion in SBF for 7 days.

15 **Figure 8** TF-XRD patterns of the specimen surfaces after NaOH treatment and  
16 subsequent immersion in SBF for 7 days.

1  
2  
3  
4  
5  
6  
7  
8  
9  
10  
11  
12  
13  
14  
15  
16  
17  
18  
19  
20  
21  
22  
23  
24  
25  
26  
27  
28  
29  
30  
31  
32  
33  
34  
35  
36  
37  
38  
39  
40  
41  
42  
43  
44  
45  
46  
47  
48  
49  
50  
51  
52  
53  
54  
55  
56  
57  
58  
59  
60  
61  
62  
63  
64  
65

1 **Figure 9** (Ca or P)/(Ti+Zr) molar ratios of the specimen surfaces with Zr content of  
2  $\geq 60$  atom% after soaking in SBF for 7 days, which were determined by EDX  
3 quantitative analyses (n=3).

4 **Figure 10** SEM images of the specimen surfaces after NaOH treatment and  
5 subsequent immersion in SBF for 7 days, which were attached and detached with an  
6 adhesive tape 5 times.

Before NaOH treatment

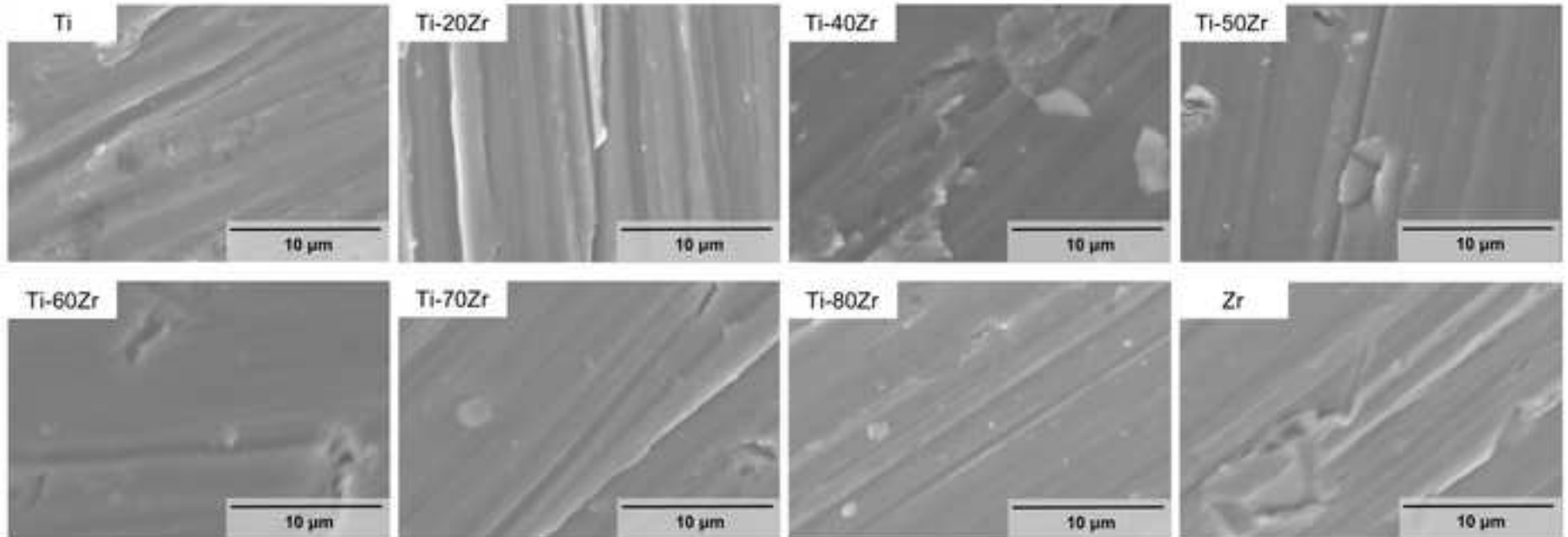


Fig. 1

After NaOH treatment

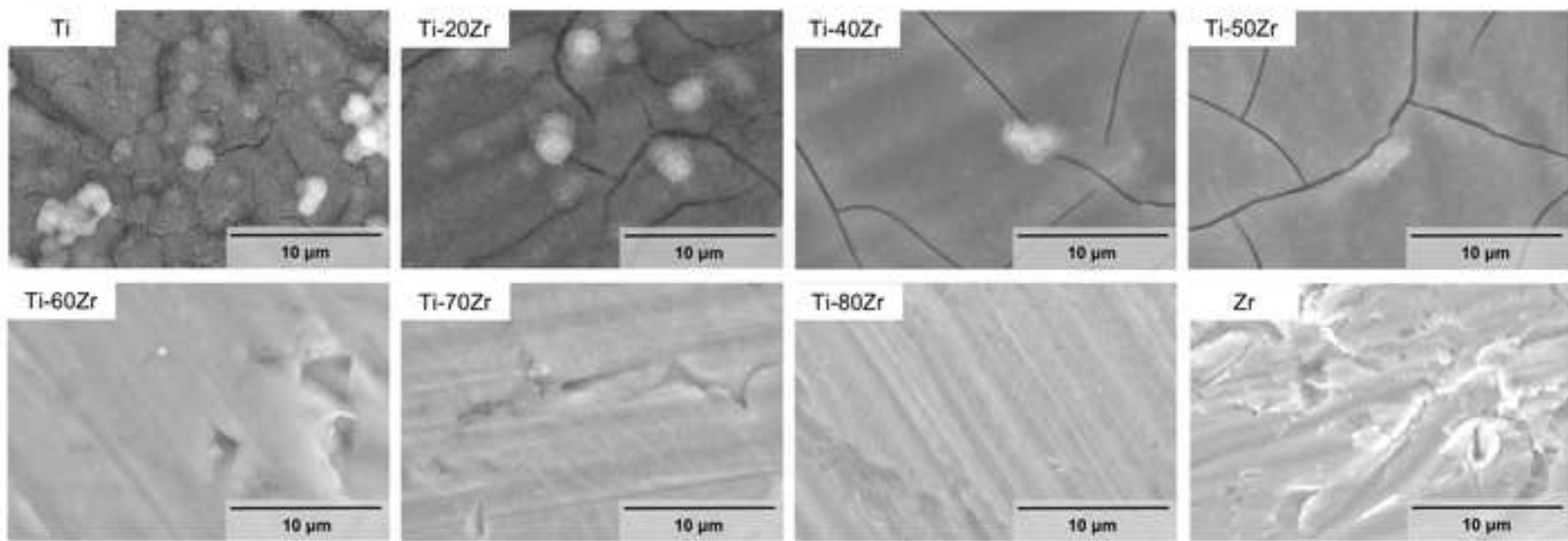


Fig. 1 (Continued)

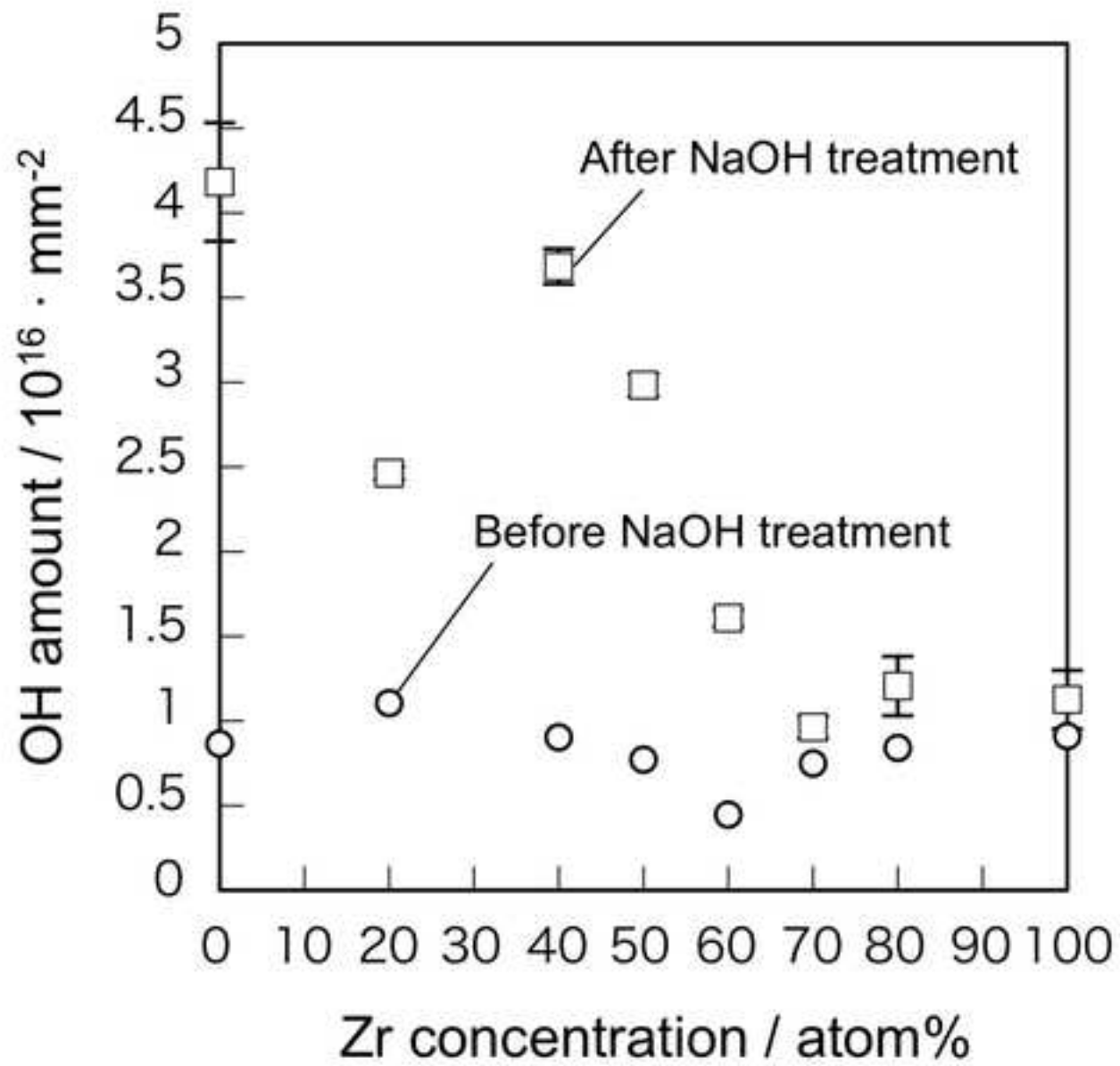


Fig. 2

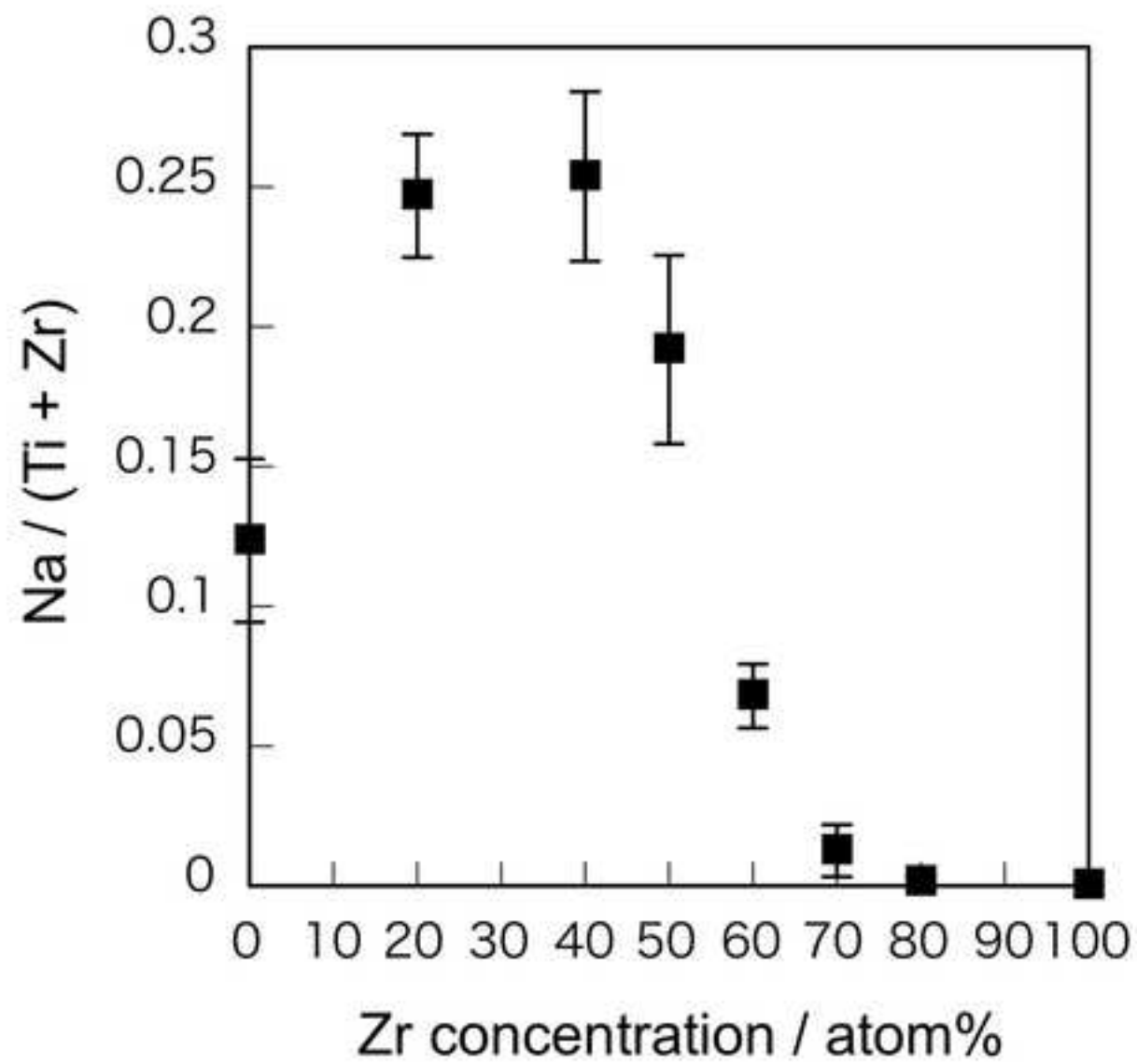


Fig. 3

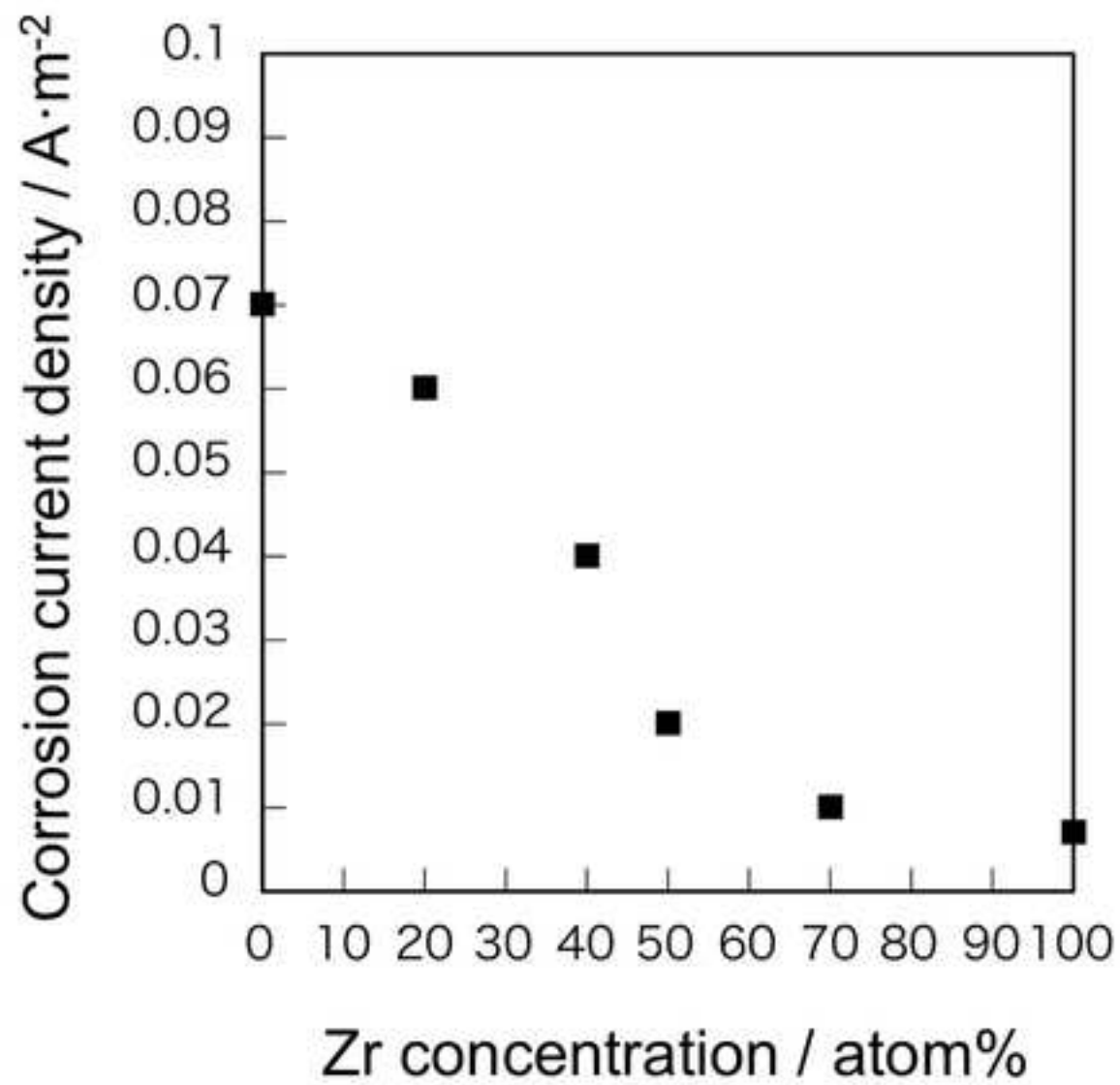


Fig. 4



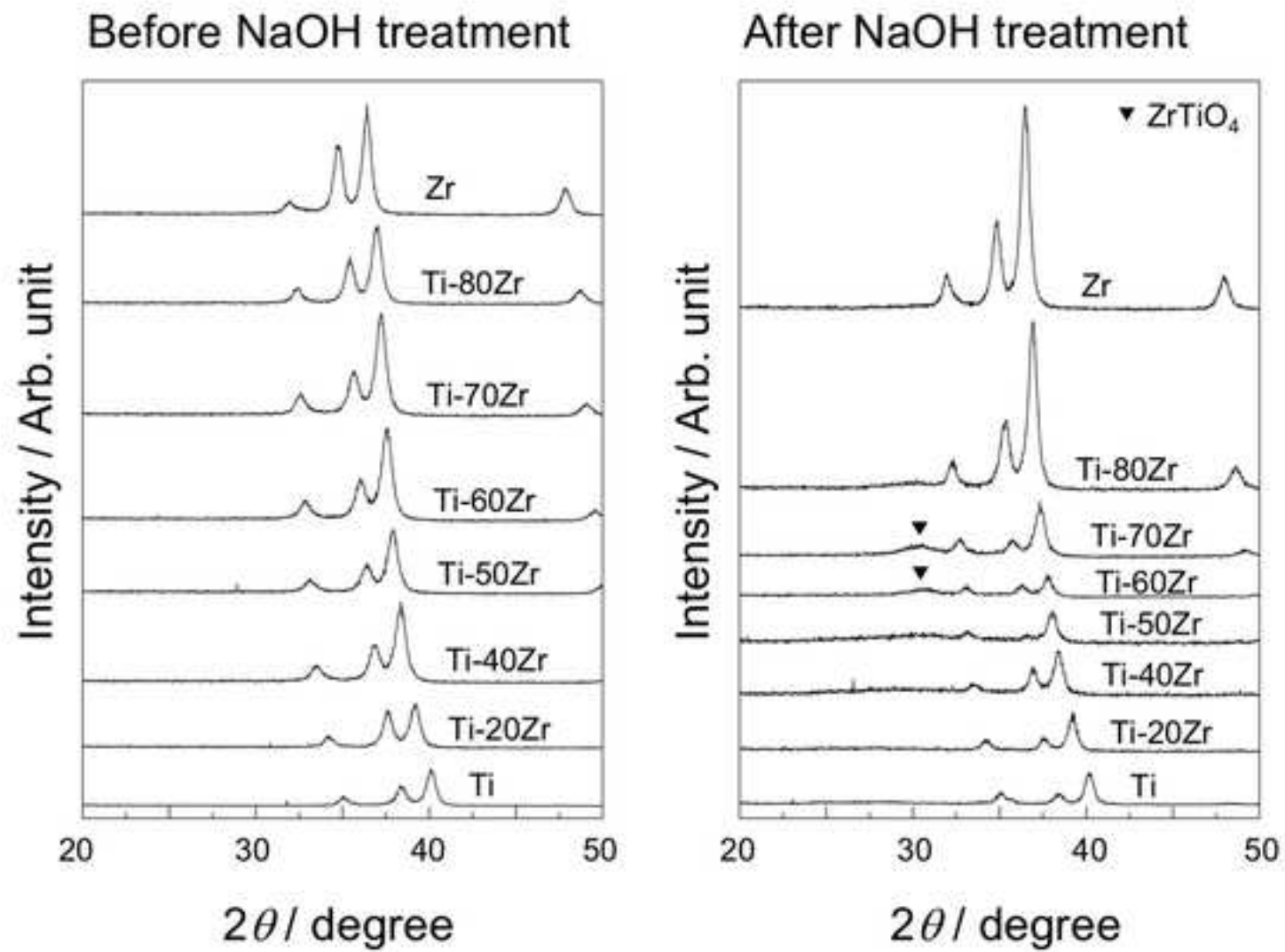


Fig. 5

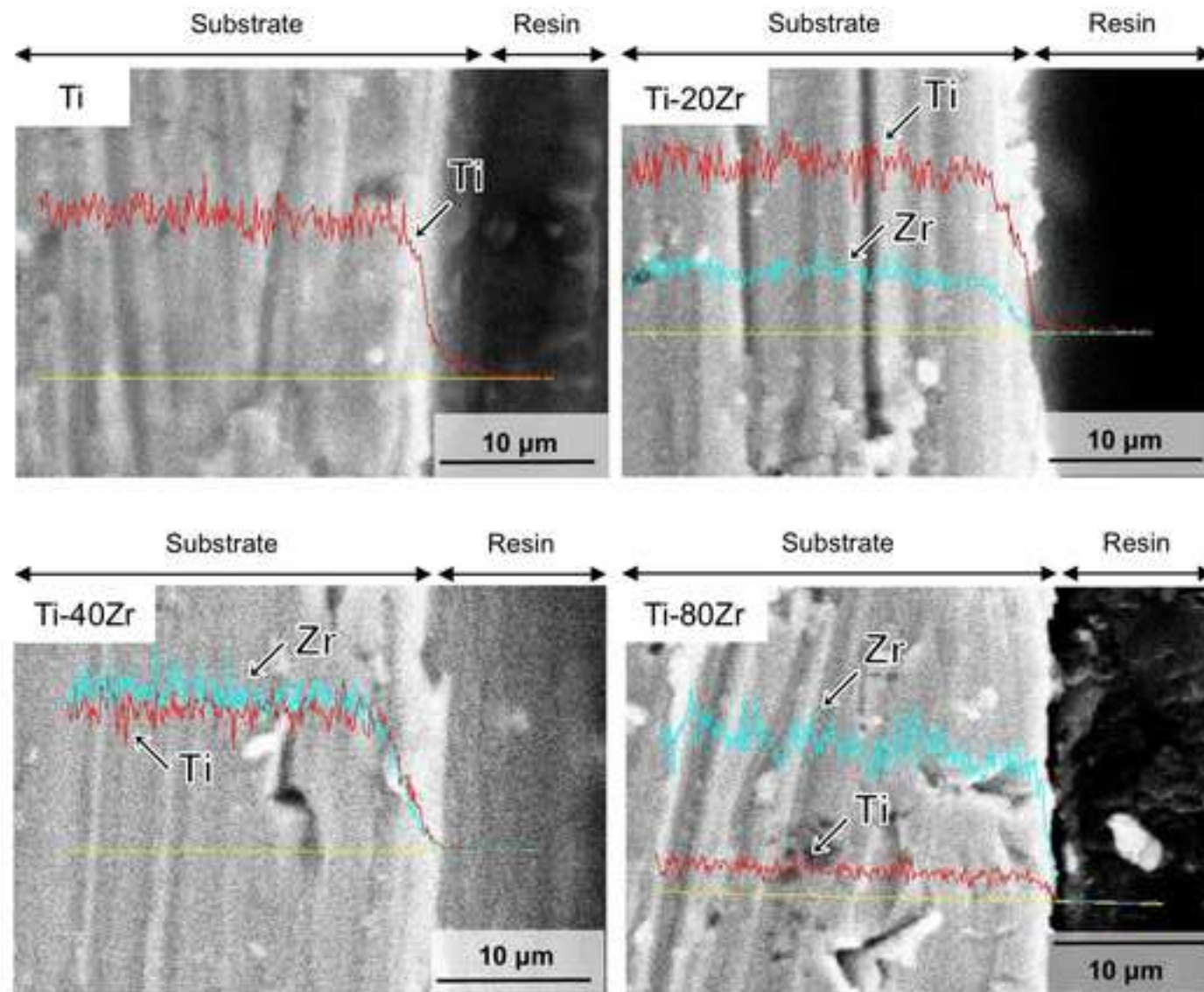


Fig. 6

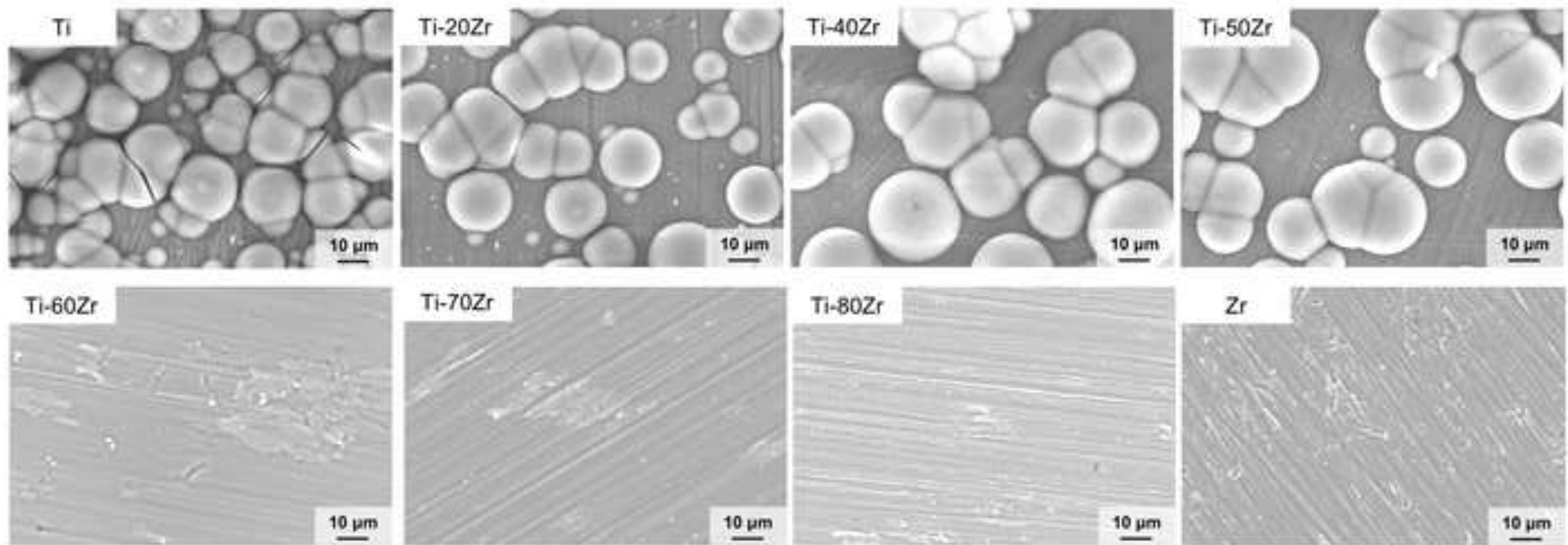


Fig. 7

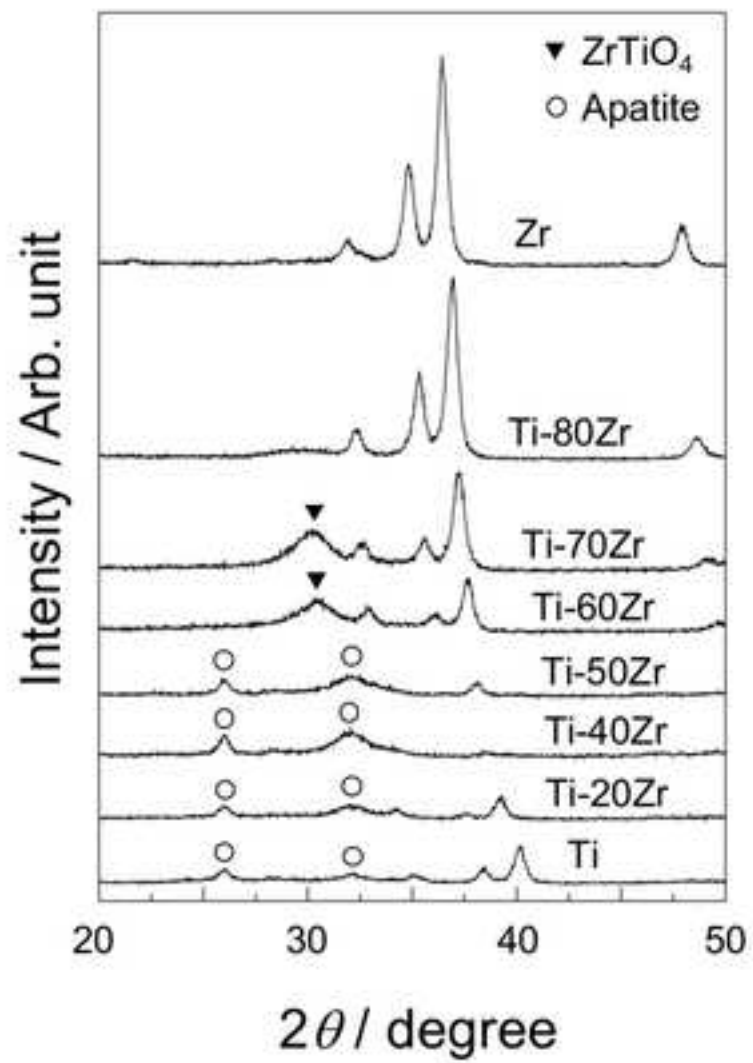


Fig. 8

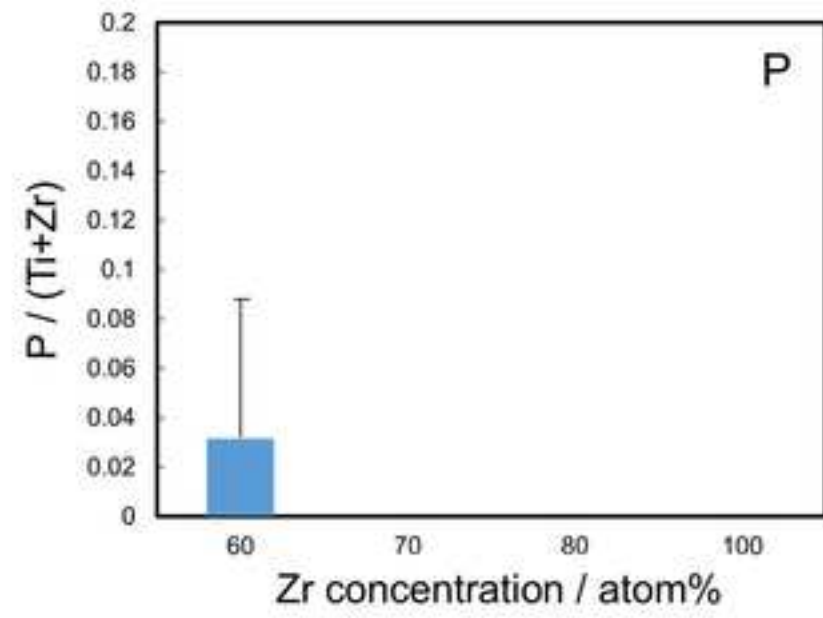
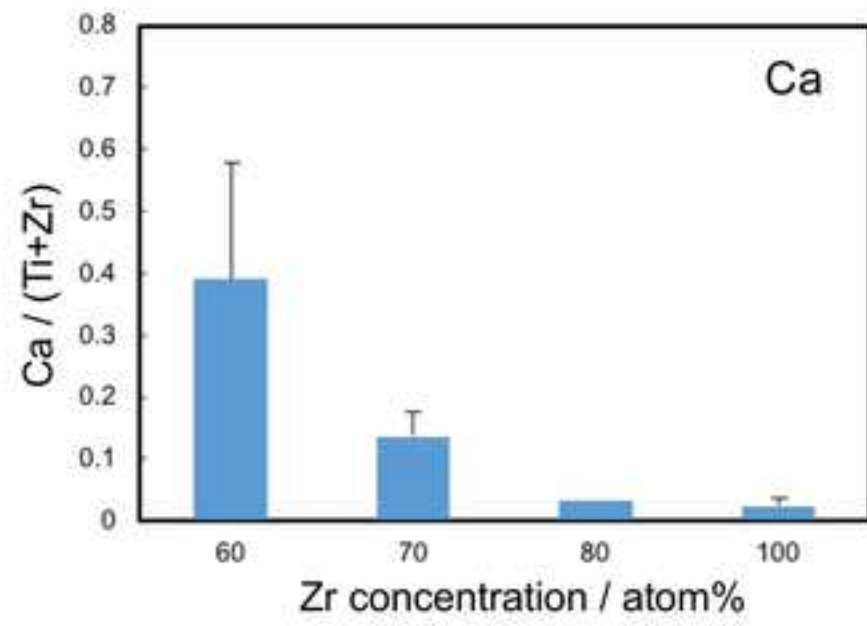


Fig. 9

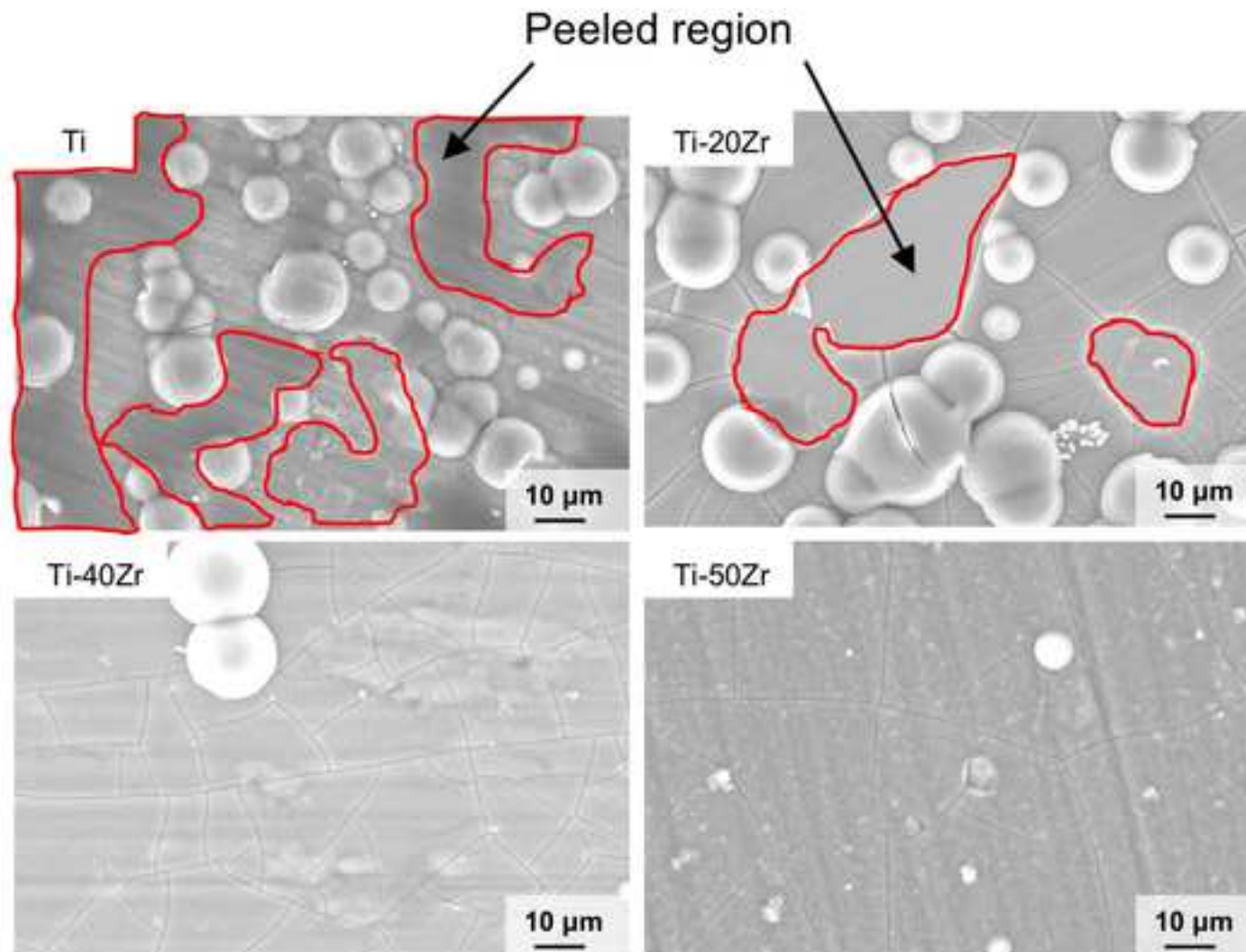


Fig. 10

